Interconnected Hierarchical ZSM-5 with Tunable Acidity Prepared by a Dealumination−Realumination Process: A Superior MTP Catalyst

Junjie Li,[†] Min Liu,[*,†] Xinwen Guo,[†] Shutao Xu,[‡] Yingxu Wei,[‡] Zhongmin Liu,[‡] and Chunshan Song[*,†,§]

[†]State Key Laboratory of Fine Chemicals, PSU-DUT Joint Center for Energy Research, School of Chemical Engineering, Dalian University of Technology, Dalian 116024, P. R. China

[‡]State Key Laboratory of Catalysis, Dalian Institute of Chemical Physics, Chinese Academy of Sciences, Dalian 116023, P. R. China

[§]Department of Energy and Mineral Engineering, EMS Energy Institute, PSU-DUT Joint Center for Energy Research, Pennsylvania State University, University Park 16802, Pennsylvania, United States

S *Supporting Information*

ABSTRACT: ZSM-5 that uses TPAOH as a template has an Al-rich exterior and defective Si-rich interior; thus, a simple base leaching selectively removed the Si-rich interior while the Al-rich exterior was protected. This catalyst showed no change in stability comparing with parent ZSM-5 during the MTP reaction that was attributed to the enclosed hollow structure and richly acidic outer shell. A preliminary fluorination, however, both removed defective Si-sites and caused distortion in tetrahedral aluminum that made the outer shell susceptible to alkaline treatment. These distorted tetrahedral Al were mostly leached out by NaOH in 1 min. Furthermore, aluminum in the filtrate was slowly redeposited onto the zeolite, serving as external pore-directing agents to control silicon dissolution from the Si-rich interior. This dealumination−realumination alkaline treatment process led to a higher solid yield and a uniform opened-mesopore structure with mesopores around 13 nm in diameter. This material was characterized by SEM, TEM, N_2 adsorption, and mercury porosimetry. In addition, NH_3-TPD, OH-IR, ^{27}Al MAS NMR, and ^1H MAS NMR results demonstrated that the reinserted Al were unlike the framework Al, contributing less to acidity. The dealumination−realumination process, therefore, was also capable of tuning the acidity of the mesoporous ZSM-5. This mesoporous catalyst exhibited a longer lifetime and a higher propylene selectivity than other catalysts with an enclosed mesopore structure.

KEYWORDS: *Al-zoned ZSM-5, enclosed hollow structure, distorted tetrahedral Al, dealumination−realumination process, reinserted Al, interconnected mesopore structure, MTP*
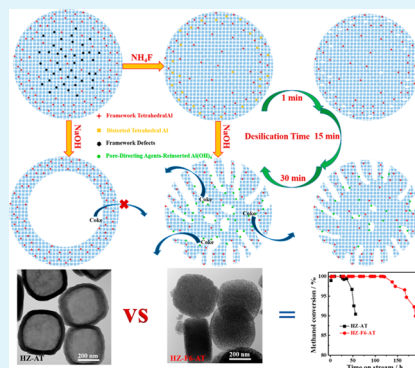
1. INTRODUCTION

Methanol conversion has received wide attention for its capability to enable feedstock replacement for conventional crude-oil-based chemical processes.[1] In the methanol- or syngas-based process, the MTP reaction is considered as a promising approach for propylene production, which can satisfy the quickly growing demand of propylene derivatives, such as polypropylene. Crude oil serves as the main resource for propylene production via steam cracking of naphtha, and the MTP process could provide an alternative as crude oil supplies decline.[2−5] Developing catalysts with a higher propylene selectivity and longer lifetime are the major enablers for MTP technology.[6−9] Zeolites with a well-defined microporous structure, strong acidity, and high hydrothermal stability have been widely tested for the MTP reaction, including ZSM-5,[3−8] ZSM-11,[10] ZSM-22,[11−15] and Beta.[16−18] ZSM-5′s three-dimensional pore structure, with straight channels (5.3 × 5.6 Å) and intersecting zigzag channels (5.1 × 5.5 Å), is the optimum catalyst for the MTP reaction. Generally, porosity and acidity are considered to be the main factors which influence product

selectivity and stability.[2,3,19,20] Lurgi, Inc. used highly siliceous H-ZSM-5 for maximizing propylene yield.[21] Rapid deactivation attributed to coke deposition over outer surface or active sites; however, it limits the development of practical MTP processes.[2,9,22,23] Recently, numerous studies demonstrated the importance of a secondary network of meso- and/or macropores,[24−27] which can be created through dealumination or desilication strategies.[28−31] Base leaching is a simple but versatile postsynthesis treatment that differs from a common dealumination method, as silicon, rather than aluminum, is extracted from the zeolite matrix.[32] The feature of mesoporous structure, including pore diameter, distribution, and connectivity, is impacted by the Si/Al ratio, Al distribution, and defect-site distribution as well as the temperature and concentration of the alkaline solution.[9,22,33−37] Selective

desilication also brings substantial alterations to acidic properties that may greatly influence catalytic performance.[32,38,39]

Pioneering work by Groen et al. showed that ZSM-5 with a Si/Al ratio range of 25−50 is optimal for generating a uniform mesopore structure.[32] At higher Si/Al ratios, limited protection by less Al led to excessive Si leaching, thus, larger mesopores and lower product yields were obtained. Controllable dissolution was achieved by incorporating external pore-directing agents $(Al(OH)_4^-, Ga(OH)_4^-, or TPA^+)$ in the alkaline medium.[40−42] For ZSM-5 with a higher amount of Al, restrained Si removal due to excessive protection by a larger amount of Al resulted in a less mesoporous structure, though sequential treatments can lead to mesopore growth.[32,43] Defective Si-sites seem more sensitive to OH^- leaching compared with framework Si. Fluoride-mediated ZSM-5, therefore, showed higher stability in alkaline solution than conventional ZSM-5, which attributed to less defect sites.[37,44] Several studies have reported that NH_4F modification preferentially removed defective Si sites.[44,45] Our group found that fluorination of ZSM-5 by NH_4F only slightly changed the bulk Si/Al ratio, but led to a higher framework Si/Al ratio by ^{29}Si MAS NMR.[46] ^{27}Al MAS NMR showed the peak at 55.5 ppm shifted to ~52 ppm and widened after NH_4F treatment; the shift has been attributed to the formation of distorted tetrahedral Al by other groups.[43,45] ZSM-5 that uses TPAOH as its template has an Al-rich exterior and defective Si-rich interior,[47] and thus, it assembled the alkaline treatment difficulties of Al-rich and Si-rich crystals even though it has an optimal Si/Al ratio for desilication. A single NaOH treatment led to a hollow structure rather than a uniform mesoporous structure. This was attributed to selective removal of the inner portion, whereas the outer surface was unaffected due to excessive protection of a higher amount of aluminum.[34,36,48] Creating an interconnected mesoporous structure into Al-zoned ZSM-5 has never been accomplished, and few studies have modulated acid properties during alkaline treatment by a controllable dealumination−realumination process.

Hence, this paper was undertaken to introduce an interconnected mesoporous structure into Al-zoned ZSM-5, which had a bulk Si/Al ratio of 37 but a lower external Si/Al ratio of 14, by dealumination−realumination process during alkaline treatment. SEM, TEM, N_2 adsorption, and Hg intrusion results were used to characterize the mesopore-size, distribution, and connectivity. Also, the variation of acid properties after the dealumination−realumination process was characterized by NH_3-TPD, ^{27}Al MAS NMR, OH-IR, and ^1H MAS NMR techniques. Different catalysts with various mesoporous structures as well as acidities were evaluated in a methanol-to-propylene reaction. This method shows great potential for designing superior MTP catalysts with higher activity, selectivity, and stability.

2. EXPERIMENTAL SECTION

2.1. Catalyst Preparation. Al-zoned ZSM-5 was synthesized as follows. Tetraethyl orthosilicate was poured into a liquor-containing water and TPAOH, and the resulting solution was hydrolyzed at 308 K for 8 h. A solution containing aluminum nitrate and sodium hydroxide was then added into silica gel and stirred for 90 min. This mother gel was poured into a Teflon-lined stainless-steel autoclave and crystallized at 443 K for 24 h. The chemical composition of the final gel was $80:1:20:4:4800\ SiO_2/Al_2O_3/TPAOH/Na_2O/H_2O$. Al-zoned NaZ was obtained by calcination at 813 K for 6 h.

The fluorination was operated by impregnating 10 g of Na-ZSM-5 with 200 mL of NH_4F solution (0.02, 0.04, 0.06, and 0.08 mol/L). The samples were vigorously stirred at 303 K for 10 h, dried at 373 K for 12 h, and calcined at 873 K for 6 h. They are abbreviated as NaZ-F2, NaZ-F4, NaZ-F6, and NaZ-F8, respectively. Alkaline-treated ZSM-5 was prepared by treating NaZ, NaZ-F2, NaZ-F4, NaZ-F6, and NaZ-F8 with NaOH solution (0.2 mol/L, with a liquid−solid ratio of 30 cm³/g) at 353 K. After 30 min, the slurry in the beaker was placed in an ice-water bath, and the solid was collected by centrifugation, washed, and dried for 12 h at 373 K. Then, the samples NaZ-AT, NaZ-F2-AT, NaZ-F4-AT, NaZ-F6-AT, and NaZ-F8-AT were calcined at 813 K for 4 h. The ammonium form of NaZ, NaZ-F6, NaZ-AT, NaZ-F2-AT, NaZ-F4-AT, NaZ-F6-AT, and NaZ-F8-AT were obtained by three repeated ion exchanges with 1.0 mol/L NH_4NO_3 solution at 353 K for 1.5 h. The product was received by centrifugation, washing, and drying for 12 h at 373 K. HZ, HZ-F6, HZ-AT, HZ-F2-AT, HZ-F4-AT, HZ-F6-AT, and HZ-F8-AT were obtained after calcination of the ammonium form samples at 813 K for 4 h.

2.2. Catalyst Characterization. An IGAKU D/Max 2400 apparatus, which was equipped with Cu Kα X-radiation, was used to characterize the XRD patterns of various catalysts. SEM images were received on a cold-field emission Hitachi SU8200 instrument with an acceleration voltage of 5 kV. TEM was performed over Tecnai G2 20 S-twin apparatus with an acceleration voltage of 200 kV. Higher-resolution TEM images were performed on a JEM-2100F apparatus. TEM samples were prepared by dipping ethanol solutions of samples onto the carbon-coated copper grids and drying at ambient conditions. N_2 adsorption−desorption results were obtained on a Quantachrome autosorb analyzer. The powder was degassed in vacuum at 573 K for 8 h before measurement. The BET surface area was calculated by the BET method. Mercury-intrusion porosimetry was performed on a Micromeritics Autopore IV 9510 to characterize the mesoporous structure. Elemental analysis was conducted over a PerkinElmer OPTIMA 2000DV apparatus. XRF spectroscopy was used to analyze the elemental contents of different samples on a SRS-3400 apparatus. TG-DTA results were received on a SDT Q600 apparatus from 298 K to 1073 K with a heating rate of 10 K/min in air. XPS measurements were obtained on an Escalab 250 apparatus.

NH_3 procedural desorption was taken on a CHEMBET 3000 chemical absorber. Approximately 100 mg of sample with 20−40 mesh was exposed to mixed gas (8% NH_3 in He) for 30 min after it was pretreated at 773 K for 1 h and cooled to 393 K. Then, helium purging at 393 K for 1 h was used to remove physically adsorbed NH_3. The TPD plot was recorded with a heating rate of 10 K/min from 393 to 923 K that was detected by gas chromatography equipped with TCD. The OH-IR spectra were collected on an EQUINOX55 apparatus from Bruker, and the analysis pellet was prepared by adding KBr. Before testing, all of the samples were heated at 573 K under vacuum (~1×10^{-5} Torr) for 4 h. The presented spectra have the background spectrum subtracted.

^{29}Si, ^{27}Al, and ^1H MAS NMR results were taken on a 600 MHz Bruker Avance III equipped with a 4 mm MAS probe. ^{29}Si MAS NMR spectra were performed using a high-power proton that was decoupled with a spinning rate of 10 kHz. The chemical shift was received by reference to 4,4-dimethyl-4-silapentanesulfonate sodium (DSS). ^{27}Al MAS NMR spectra were performed by using a one-pulse sequence with a spinning rate of 12 kHz. The chemical shift was with reference to $(NH_4)Al(SO_4)_2 \cdot 12H_2O$ at −0.4 ppm. Before ^1H MAS NMR measurements, the samples were dehydrated at 693 K under a pressure below 10^{-3} Pa for 20 h.

2.3. Catalytic Tests. Methanol conversion to propylene was performed in a fixed-bed continuous-flow reactor (with a stainless-steel tube of 8 mm I.D.). In a typical run, 1 g of catalyst (size 10−20 mesh) was put in the flat-temperature zone of the reactor tube, and the methanol/water mixture (molar ratio 1:1) was injected by a Lab Alliance Series II pump to provide a methanol WHSV of 3.0 h^{-1}. Prior to testing, the catalyst was activated in situ at 773 K for an hour. Then the mixture of CH_3OH and H_2O was pumped into the reactor. The tests were conducted at 773 K under atmospheric pressure, and a gas chromatograph equipped with a FID detector and a 30 m HP-PLOTQ

capillary column was used to analyze gas products. The methanol in liquid products was detected by a GC equipped with FID and a 2 m HayeSep Q packing column. Methanol as well as dimethyl ether were used as reactants for the conversion measurement.

3. RESULTS AND DISCUSSION

3.1. Physicochemical Properties. All of the catalysts display a typical MFI topology, and no amorphous phase components or impurities are detected in the XRD patterns shown in Figure 1. The crystallinity of different samples was
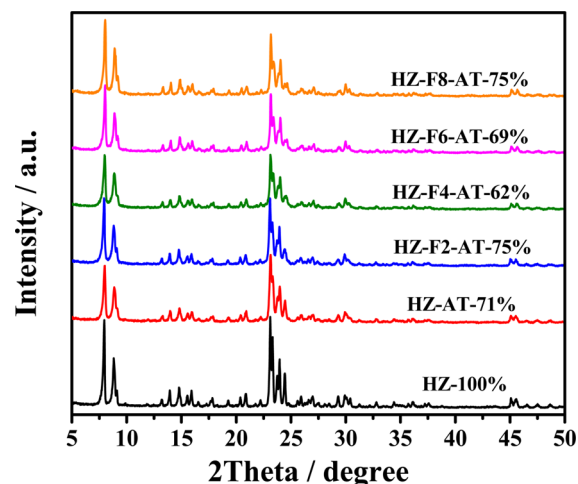

Figure 1. XRD patterns of catalysts via different treatment methods.

calculated from the double peak at around 8° and the triple peak at around 22° based on the parent HZ, which shows 100% crystallinity in Figure 1. HZ-AT, HZ-F2-AT, HZ-F4-AT, HZ-F6-AT, and HZ-F8-AT show various crystallinities of 71, 75, 62, 69, and 75%, respectively. It can be concluded that crystallinity reduces after NaOH treatment, which is attributed to the destruction of the microporous structure during the alkaline treatment. The textual and chemical properties of the samples are summarized in Table 1. Parent HZ shows a Si/Al ratio of 37, and HZ-F6 via 0.06 M NH_4F modification has a similar Si/Al ratio of 35; it shows a higher solid yield of 96% because of selective removal of the defective Si sites. Single NaOH-treated HZ-AT leads to a lower yield of 42% and a Si/Al ratio of 18. Samples treated through a sequential fluorination and alkaline

treatment (HZ-F2-AT, HZ-F4-AT, HZ-F6-AT, and HZ-F8-AT) show a higher solid yield than HZ-AT.

SEM and TEM were employed to characterize the morphologies and porous structure of the parent and modified samples. Figure 2a shows that our synthesis procedure resulted in 450 nm monodispersed particles, with an Al-rich external surface (Si/Al = 14) relative to that of bulk Si/Al as determined by XPS. According to the SEM images, these samples can be divided into two types. Samples HZ, HZ-AT, and HZ-F2-AT exhibit similar smooth external surfaces, whereas samples HZ-F4-AT, HZ-F6-AT, and HZ-F8-AT display rough surfaces. Figure 3 shows TEM images of samples via various treatments that clearly demonstrate the distinctions of various crystals. HZ in Figure 3a shows typical microporous ZSM-5 with little intracrystal mesopore structure. HZ-AT in Figure 3b displays a hollow structure with an intact microporous shell, which is in agreement with the smooth surface from SEM in Figure 2b. HZ-F2-AT exhibits a mesoporous structure instead of cavities; however, the dark shell in Figure 3c and the relatively smooth exterior in Figure 2c partly suggest an enclosed mesoporous structure. Figure 3d shows some particles with an annular hollow structure, which is corroborated by the SEM morphologies in Figure 2d. The microporous shell completely disappears for the HZ-F6-AT and HZ-F8-AT samples that show homogeneously distributed mesopores, and the morphology remains largely uninfluenced relative to parent HZ. Higher-magnification TEM images of HZ-F6-AT in Figure 3g,h also display uniform mesopore structures. The combined SEM and TEM analysis points to an open mesoporous structure of HZ-F6-AT and HZ-F8-AT, and further research by N_2 adsorption and mercury-intrusion was used to prove this point.

The hierarchical structures were also studied by N_2 adsorption (Figure 4a,b). Parent HZ in Figure 4a shows a type I N_2 adsorption−desorption isotherm with a micropore volume of 0.16 cm^3 g^{-1} and a surface area of 435 m^2g^{-1} (Table 1). HZ-F6 shows a lower BET surface area of 371 m^2g^{-1} compared with that of parent HZ, which corresponds to a lower microporous volume. It may be attributed to slight destruction of microporous structure. It also shows a little higher external surface area compared with that of HZ and a similar lower mesoporous volume to that of HZ. The alkaline-treated samples show type IV adsorption−desorption isotherms with enhanced uptake at higher P/P_0, and distinct hysteresis loops reveal different hierarchical porous structures. A single

Table 1. Textual and Chemical Properties of Parent and Modified Catalysts

	treatment conditions					textual data					
samples	C_{NH4F} (mol/L)	CNaOH (mol/L)	Si/Al[a]	HF[b]	yield (%)	S_{BET}[c] (m^2 g^{-1})	S_{EXT}[d] (m^2 g^{-1})	V_T[e] (cm^3 g^{-1})	V_{micro}[d] (cm^3 g^{-1})	V_{meso}[f] (cm^3 g^{-1})	V_{meso}[g] (cm^3 g^{-1})
HZ	-	-	37	-	100	435	37	0.26	0.16	0.10	0.00
HZ-AT	-	0.2	18	0.02	42	347	35	0.51	0.13	0.38	0.23
HZ-F6	0.06	-	35	-	96	371	55	0.19	0.13	0.06	-
HZ-F2-AT	0.02	0.2	23	0.07	55	379	66	0.31	0.13	0.18	-
HZ-F4-AT	0.04	0.2	25	0.08	60	408	113	0.46	0.13	0.33	-
HZ-F6-AT	0.06	0.2	26	0.09	66	419	143	0.46	0.12	0.34	0.41
HZ-F8-AT	0.08	0.2	27	0.09	68	387	117	0.37	0.11	0.26	-

[a]XRF. [b](V_{micro}/V_T)*(S_{EXT}/S_{BET}). [c]BET method. [d]t-plot. [e]P/P_0 = 0.99. [f]$V_T - V_{micro}$. [g]Mesoporous volume from mercury-intrusion method in the 20−414 MPa.
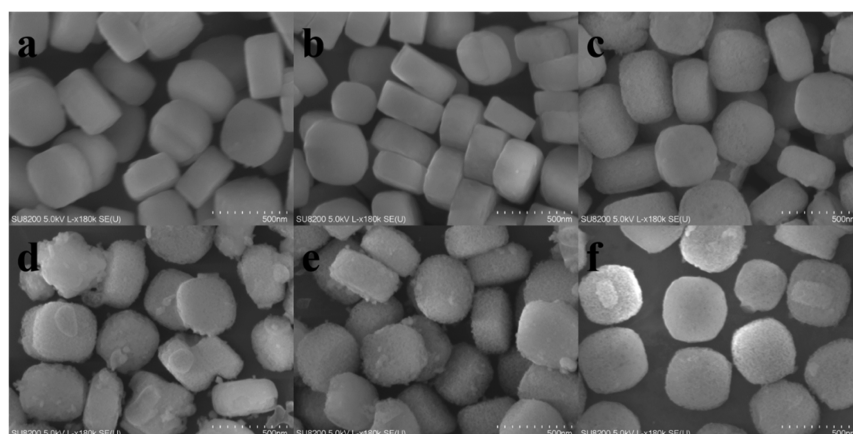
Figure 2. SEM images of (a) HZ, (b) HZ-AT, (c) HZ-F2-AT, (d) HZ-F4-AT, (e) HZ-F6-AT, and (f) HZ-F8-AT.
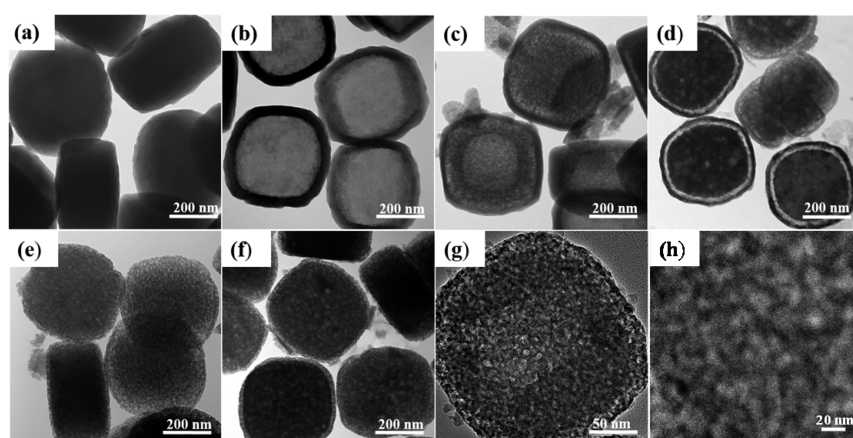

Figure 3. TEM images of (a) HZ, (b) HZ-AT, (c) HZ-F2-AT, (d) HZ-F4-AT, (e) HZ-F6-AT, and (f) HZ-F8-AT, and (g,h) higher magnification TEM images of HZ-F6-AT.

NaOH treatment (HZ-AT) leads to an apparent H2 hysteresis loop with a forced closure at $P/P_0 = 0.42$ (Figure 4a), pointing toward the existence of cavities or a mesopore structure that must be reached through entrances or micropores smaller than 4 nm. As shown in Table 1, HZ-AT has a higher total pore volume ($V_T = 0.51$ cm^3 g^{-1}) but a lower external surface area ($S_{EXT} = 35$ m^{2}g^{-1}), which suggests some extent of occluded or constricted pores. HZ-F2-AT displays a pronounced H1 hysteresis with obvious N$_2$ adsorption at a higher P/P_0, and Figure 4b exhibits a broad pore-size distribution of about 13 nm. HZ-F2-AT has a slightly higher external surface area of 66 m^{2}g^{-1}. HZ-F4-AT, HZ-F6-AT, and HZ-F8-AT show a larger adsorption at a higher pressure in Figure 4a, which suggests substantial mesopore development, and the external surface area increases from 37 to 143 m^{2}g^{-1} for HZ-F6-AT. Figure 4b shows uniform pore-size distribution centered near 13 nm.

Mercury-intrusion results were used to determine the connectivity of parent and alkaline-treated samples. Mercury cannot significantly penetrate into pores smaller than 3 nm (the highest pressure is around 414 MPa). As shown in Figure 4c, there is no intrusion of mercury for HZ, indicating a purely microporous structure. The pore distribution at around 100 nm in Figure 4d belongs to interparticle pores rather than intracrystal mesopores.[35] Distinct Hg intrusion was found for HZ-AT and HZ-F6-AT in the pressure range of 20−414 MPa in Figure 4c, correlating to pores between 4 and 80 nm. As shown in Table 1, HZ-AT has a lower Hg intrusion of 0.23 cm^3

g^{-1} compared with a higher V_{meso} of 0.38 cm^3 g^{-1} as found by N$_2$ adsorption results. Figure 4d shows a minor pore distribution at around 7 nm for HZ-AT, and the pore distribution at around 60 nm may be attributed to a crushed hollow structure at a higher pressure. HZ-F6-AT shows a larger Hg intrusion of 0.41 cm^3 g^{-1}. The intruded volume of 0.41 cm^3 g^{-1} found by Hg experiments is a little larger than V_{meso} of 0.34 cm^3 g^{-1} derived from N$_2$ adsorption results, thus suggesting an open mesopore structure. HZ-F6-AT exhibits a uniform pore distribution centered around 13 nm in Figure 4d, which was also seen with N$_2$ adsorption results. The combined analysis of TEM, SEM, N$_2$ adsorption, and Hg intrusion leads us to conclude that HZ-F6-AT has an interconnected hierarchical structure, whereas HZ-AT shows an enclosed hierarchical structure.

3.2. Pore-Forming Mechanism and Acid Properties.

^{27}Al MAS NMR, as shown in Figure 5, was performed to characterize the distortion of aluminum states. A single signal at 56 ppm and a minor signal at 0 ppm is found for HZ, indicating a high percentage of tetrahedral Al. ^{29}Si MAS NMR in Figure S1 shows a framework Si/Al ratio (41) close to that of the bulk Si/Al ratio (37). We conclude that tetrahedral Al in HZ is entirely framework Al. Very little signal is observed at 0 and 30 ppm for HZ-AT, which would be attributed to six-coordinated and five-coordinated Al, respectively. However, a broader and shifted signal at 54 ppm was detected for HZ-F6, suggesting the existence of various types of four-coordinate Al species. The
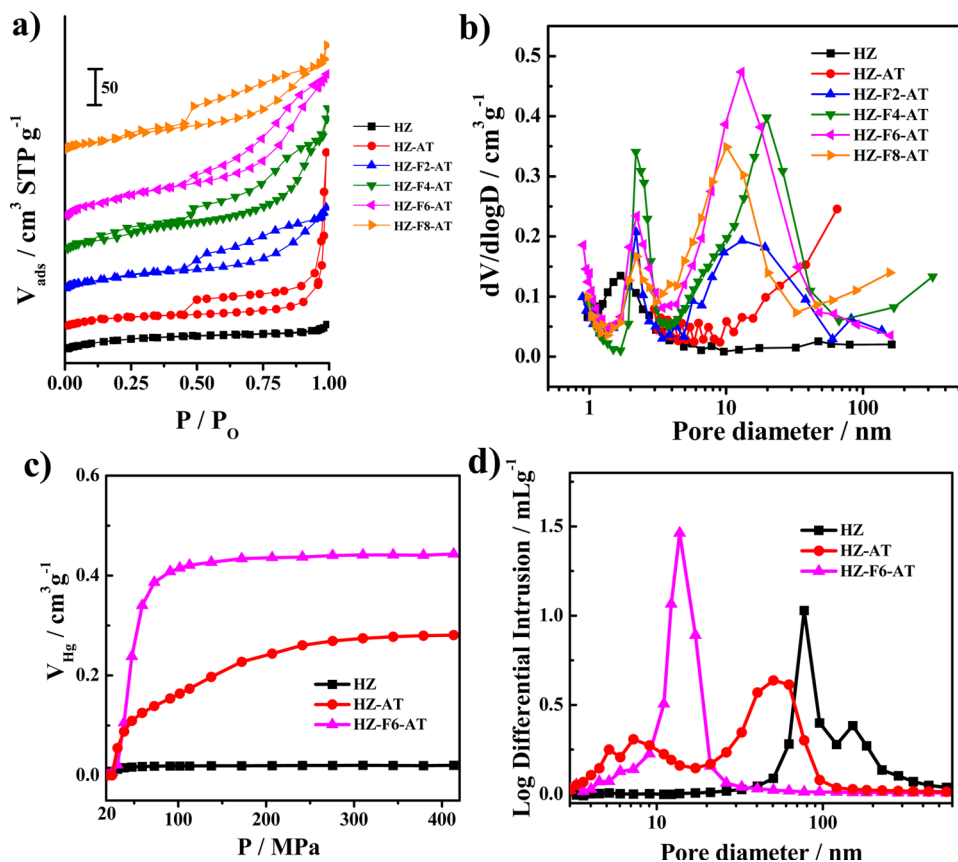
Figure 4. N$_2$ adsorption isotherms at 77 K (a) and BJH pore-size distributions (b) of parent and alkaline-treated zeolites. Mercury-intrusion curves between 20 and 414 MPa of samples with different porosity (c), and pore-size distributions derived by Hg intrusion (d).
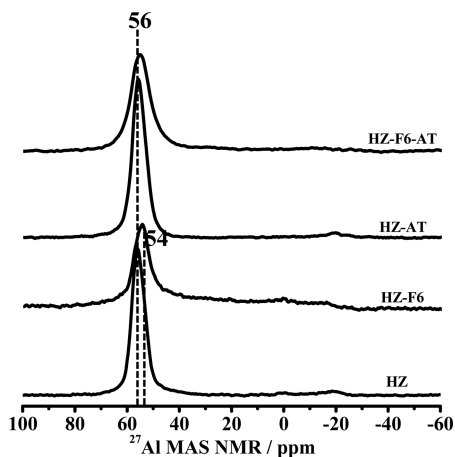

Figure 5. ^{27}Al MAS NMR spectra of zeolites via different treatment methods.

signal at 54 ppm may be related to tetrahedral Al species distorted by fluorination.[43,45] Figure S1 also exhibits a higher framework Si/Al of 80 for HZ-F6. The peak shift disappeared after NaOH treatment for HZ-F6-AT, which we attribute to the removal of distorted tetrahedral Al during alkaline treatment. ICP results determining the amount of Al in the NaOH solution will corroborate this conclusion.

Figure 6a,b show the contents of silica (Si$_{Filtrate}$) and aluminum (Al$_{Filtrate}$) in the filtrate during NaOH treatment. As shown in Figure 6a, there was less Al$_{Filtrate}$ during NaOH treatment for NaZ. Thus, we conclude that alkaline treatment

did not impact framework Al. The amount of Al$_{Filtrate}$ for NaZ-F2, NaZ-F4, NaZ-F6, and NaZ-F8, however, is several times larger than that for NaZ, and the dealumination degree reaches a maximum at 1 min. ZSM-5 with a higher Si/Al ratio, therefore, was present after 1 min of desilication. On the basis of ^{27}Al MAS NMR for HZ-F6-AT, we conclude that distorted tetrahedral Al can be leached out during the initial alkaline treatment, whereas framework tetrahedral Al remains unaffected. Thus, the negative effect of regional desilication attributed to Al-zoning can be weakened by selective dealumination in the initial stage.

The Al$_{Filtrate}$ gradually redeposited onto zeolites, and there was less aluminum in the final filtrate for all of the samples regardless of how much Al was initially leached out. Table 1 shows a lower Si/Al ratio for alkaline-treated samples compared with parent HZ, which also proves reinsertion of removed Al. As shown in Figure 6b, a significant amount of silicon is leached out by NaOH prior to 15 min for NaZ-F6, which is higher than that for the parent NaZ, because 28% of Al sites in the NaZ-F6 matrix were removed in the initial 1 min and no longer shielded their neighbor Si. The desilication rate declined after 15 min of alkaline treatment for NaZ-F6, which we attribute to the gradual redeposition of the Al$_{Filtrate}$ onto the surface of crystals. Redeposited Al suppresses excessive dissolution of the Si-rich interior by serving as external pore-directing agents. HZ-F6-AT, therefore, shows a higher solid yield of 66% in Table 1 and a uniform open mesopore structure at around 13 nm (by N$_2$ sorption results). In contrast, a larger amount of Si is leached out in the final stage for NaZ, which results in lower yield of 42% and an enclosed hierarchical structure. This is attributed to
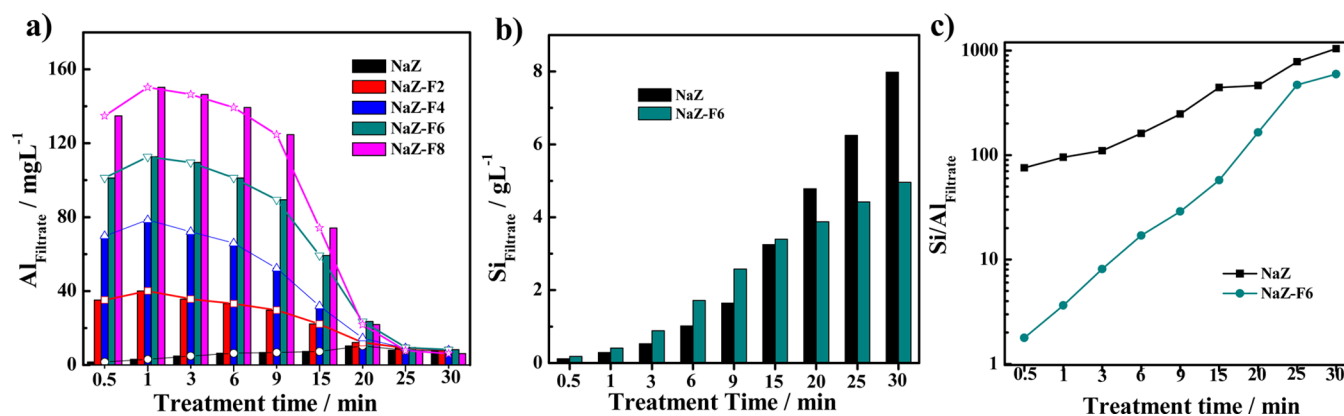
Figure 6. Variation of aluminum (a), silica (b), and Si/Al (c) in the filtrate during NaOH treatment; the treatment was carried out in a 0.2 M NaOH solution at 353 K.
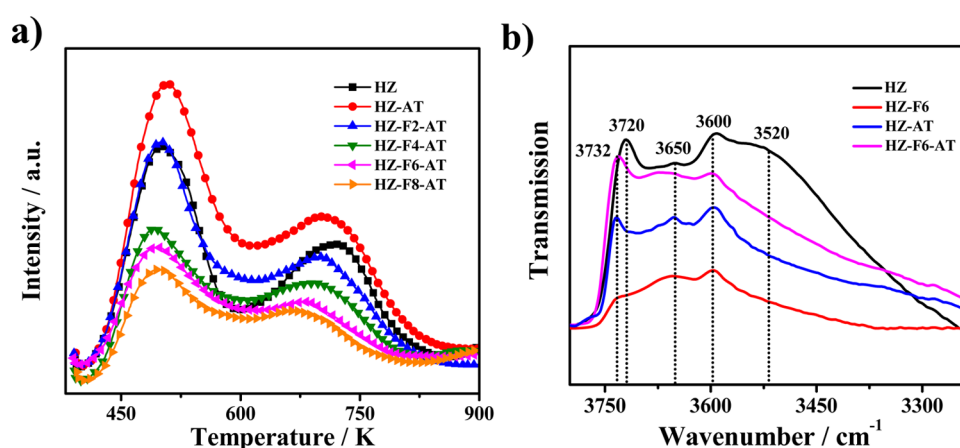

Figure 7. NH$_3$-TPD profiles (a) and IR spectra in hydroxyl vibration region (b) for H-ZSM-5 samples via different treatment methods.

excessive dissolution of the defective Si-rich interior. Table 1 shows the highest yield of 68% for HZ-F8-AT even though almost 40% of Al is extracted in the first minute. Figure 6c shows the Si/Al ratio in the filtrate (Si/Al$_{Filtrate}$) with respect to treatment duration. The initial Si/Al$_{Filtrate}$ ratio for NaZ was 75 times higher than the the Si/Al ratio for the NaZ matrix (37), and the initial ratio keeps increasing to 964 in the final solution, proving selective desilication. It is surprising, however, that the Si/Al$_{Filtrate}$ ratio for NaZ-F6 is 1.78 at 1 min, suggesting selective dealumination in the initial stage. The Si/Al$_{Filtrate}$ ratio in the final filtrate is 596, which also indicates selective desilication like for NaZ. The synergy of dealumination in the initial stage and reinsertion of Al$_{Filtrate}$ in the following stage gives rise to a uniform open-mesopore structure. The ^{27}Al spectrum of HZ-F6-AT in Figure 5 reveals only one signal at 56 ppm that represents typical four-coordinate Al, which demonstrates that reinserted Al acts as tetrahedral Al.

Figure 7a shows the NH$_3$-TPD profiles of samples with or without alkaline treatment. The two ammonium-desorption peaks at around 500 and 720 K for HZ are typically attributed to NH$_3$ desorption from weak and strong acid sites, respectively. Table 2 gives acidity amounts based on NH$_3$-TPD for different catalysts. HZ-AT exhibits a larger amount of acidity (401 μmol/g) than HZ (292 μmol/g), which is attributed to selective desilication of the Si-rich interior without impact on the outer-shell framework Al. The acidity gradually decreases as HZ-F8-AT < HZ-F6-AT < HZ-F4-AT < HZ < HZ-F2-AT, which we attribute to the dealumination–

Table 2. Acidity of Parent and Modified (Mesoporous) ZSM-5 Crystals

sample	total acidity (μmol/g)	weak acidity (μmol/g)	strong acidity (μmol/g)
HZ	292	166	126
HZ-AT	401	196	205
HZ-F2-AT	300	149	151
HZ-F4-AT	215	119	96
HZ-F6-AT	161	94	67
HZ-F8-AT	149	97	52

realumination process during NaOH treatment. Table 1 shows a lower Si/Al ratio of 26 for HZ-F6-AT, and ^{27}Al MAS NMR of HZ-F6-AT in Figure 5 displays a main signal at 56 ppm. These results point toward special tetrahedral Al that contributes less to acidity. These special Al may be assigned as reinserted Al by combining the analyses in Figure 5 and Figure 6.

Acidity changes of samples were also studied by FT-IR in the hydroxyl-stretch vibration regions in Figure 7b. There are five main IR bands in the region of 3800−3500 cm^{-1}. The first one at 3732 cm^{-1} corresponds to external free silanol groups and has a shoulder band at 3720 cm^{-1} attributed to internal (defective) silanol groups.[49] A smaller band at 3650 cm^{-1} belongs to extraframework aluminum hydroxyls. Another major band at 3600 cm^{-1} could be ascribed to Brönsted acid sites Si(OH)Al. A unique band at 3520 cm^{-1} is observed for parent

HZ, which is generally assigned to silanol nests. Both internal silanol groups and silanol nests serve as defect sites. Fluorination significantly decreases the intensities at 3720 and 3520 cm^{-1}, which is indicative of selective defect removal. Lower intensity of the band at 3600 cm^{-1} for HZ-F6 suggests less framework Al compared to HZ, which is agreement with the distortion of tetrahedral Al in ^{27}Al MAS NMR and the higher framework Si/Al ratio in ^{29}Si MAS NMR. As shown in Figure 7b, two bands at 3720 and 3520 cm^{-1} also disappear for HZ-AT, which confirms selective leaching of defective Si-sites by NaOH. HZ-AT, additionally, has a larger intensity at 3600 cm^{-1}, which is agreement with a larger amount of acid sites. A larger band at 3732 cm^{-1} is detected for HZ-F6-AT, which demonstrates a larger amount of terminal silanol groups, in accordance with a higher external surface area (S_{EXT} = 143 m^{2}g^{-1}) from N$_2$ adsorption results. A lower intensity band at 3600 cm^{-1} compared to that of HZ suggests special tetrahedral Al species for HZ-F6-AT.

^{1}H MAS NMR experiments, as shown in Figure 8, show three main resonances with chemical shifts of 1.8, 2.3, and 3.8
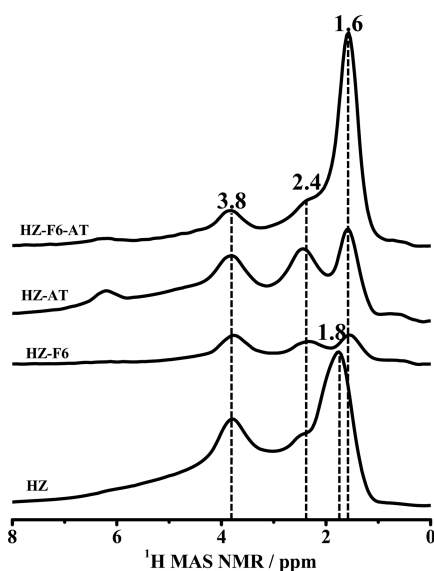

Figure 8. ^{1}H MAS NMR spectra of HZSM-5 via different treatment methods.

ppm. The peak at around 1.8 ppm is assigned to terminal silanol groups or Si−OH at structure defects, whereas the peaks at 2.3 and 3.8 ppm are attributed to silanol groups at nonframework Al species and bridge hydroxyl species (Brönsted acid sites), respectively.[50,51] As shown in Figure 8, HZ has a higher intensity at 1.8 ppm, attributed to a greater concentration of defect silanol groups or external silanol groups. A lower intensity at 1.6 ppm was detected for fluorinated HZ-F6. Fluorination is accepted to selectively remove defective Si sites without influencing external silanol groups, and Table 1 shows a similar external surface area compared to that of HZ. Thus, it can be concluded that the signal at 1.6 ppm belongs to external surface Si−OH, whereas a signal at 1.8 ppm is assigned to defective silanol groups. A larger intensity at 1.6 ppm for HZ-AT and HZ-F6-AT also corroborates these assignments, because NaOH treatment selectively removes defective Si-sites and gives rise to a larger external surface area that leads to less defective silanol groups and more terminal silanol groups. HZ-F6-AT shows a larger

intensity at 1.6 ppm compared with that of HZ-AT, which is indicative of a higher external surface area. A lower intensity at 3.8 ppm for HZ-F6-AT suggests less Brönsted acid sites compared with HZ, which we ascribe to special Al species that contribute less to acidity, as suggested by NH$_3$-TPD, ^{27}Al MAS NMR ,and OH-IR results.

3.3. Catalytic Performance for MTP Reaction. Catalysts were evaluated on a continuous flow fix-bed reaction at 773 K. Figure 9 presents the methanol conversion versus time on
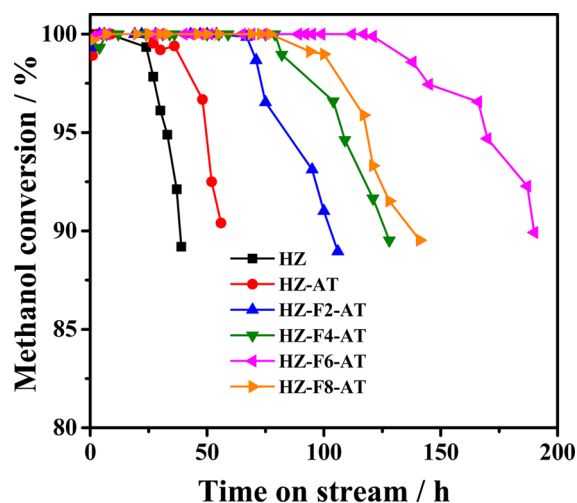

Figure 9. Variation of methanol conversion with the time-on-stream (TOS) over parent and alkaline-treated samples. (Reaction conditions: T = 773 K, P = 1 atm, WHSV = 3 h^{-1}, H$_2$O/CH$_3$OH = 1:1).

stream for various catalysts. All of the six catalysts reached 100% methanol conversion initially. The lifetime for which methanol conversion remains higher than 90% varies among the samples. As shown in Figure 9, methanol conversion drops below 90% after 38 h of reaction over HZ. The poor diffusion efficiency and rich acidic outer surface led to quick coke deposition on the external surface. HZ-AT shows an indistinct stability increase of 18 h compared to HZ because a single alkaline treatment leads to an enclosed core−shell structure, which contributes less to the diffusion of coke precursor. Furthermore, the unchanged Al-rich shell and greater acidity also accelerates the deactivation rate.[5,7,22,45] Though a shorter diffusion path and selective removal of defect sites may explain the 18 h longer lifetime, several studies confirm the significant effects of framework defects on catalytic performance.[49,51,52] The four catalysts prepared via sequential fluorination and desilication showed much higher stability. Their lifespans follow the order HZ-F6-AT > HZ-F8-AT > HZ-F4-AT > HZ-F2-AT. HZ-F2-AT shows a 50 h longer lifetime compared to HZ-AT, which we attribute to an enhanced diffusion rate and reduced acidity. HZ-F6-AT displays the longest lifetime, 195 h, almost five times longer than HZ because of an interconnected hierarchical structure and a suitable acidity.[2,5,7] HZ-F8-AT shows a relatively shorter lifetime as HZ-F6-AT in spite of a similar porous structure, possibly due to less acidity. Figure S2 shows coke deposition after deactivation of samples. HZ-F6-AT shows a similar amount of coke deposition as HZ and HZ-AT in spite of its longer lifespan, corroborating the lower coke deposition rate that occurs due to the interconnected mesoporous structure and suitable acidity.
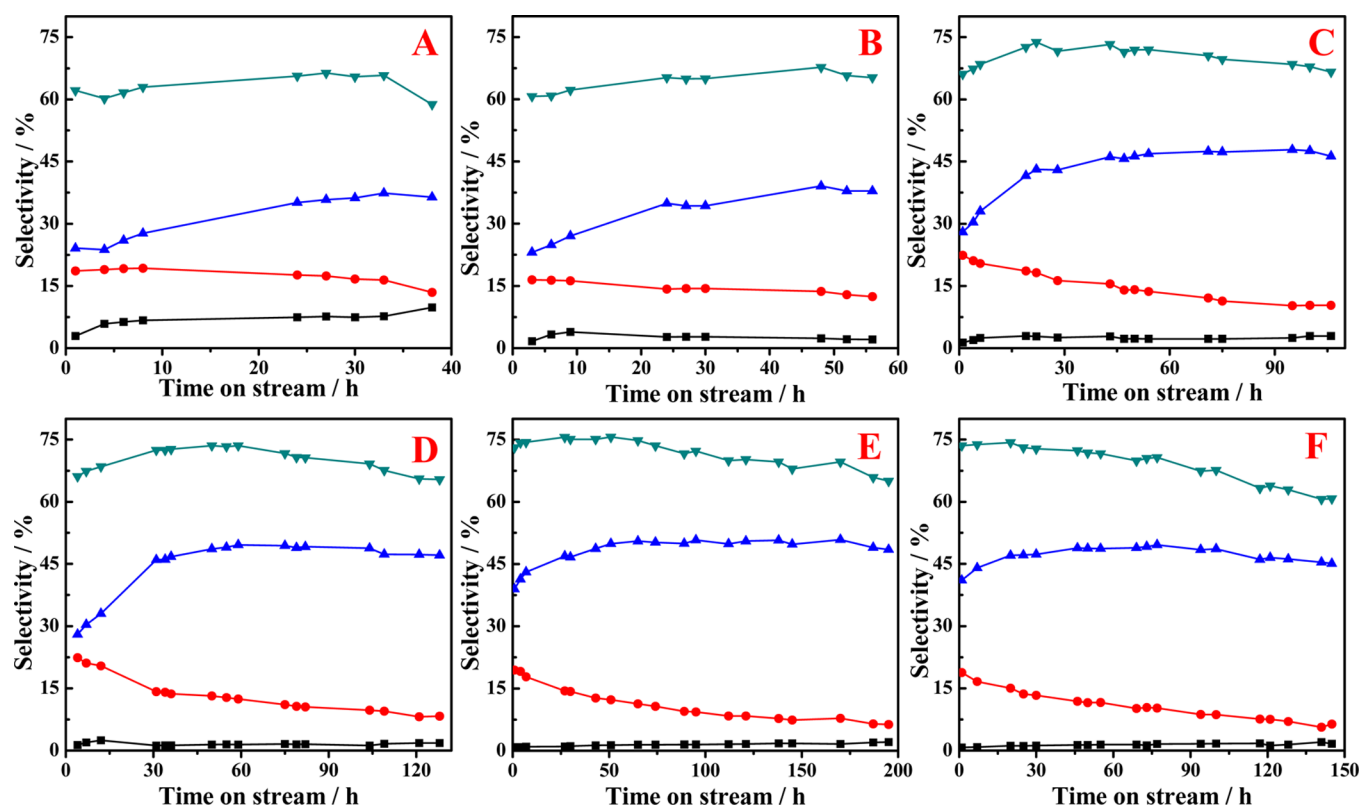
Figure 10. Product selectivity of the samples via different treatment methods for MTP reaction. (A) HZ; (B) HZ-AT; (C) HZ-F2-AT; (D) HZ-F4-AT; (E) HZ-F6-AT; (F) HZ-F8-AT. Methane selectivity (■); Ethylene selectivity (red ●); Propylene Selectivity (blue ▲); $C_2^=-C_4^=$ Selectivity (green ▼).

Changes of methane, ethylene, propylene, and $C_2^=-C_4^=$ selectivity versus time on stream are shown in Figure 10. Parent HZ shows an increasing propylene selectivity from 24.1 to 36.4%; ethylene selectivity displays adverse variation from 18.6 to 13.4%, and the methane selectivity is much higher than other samples as it grows from 2.9 to 9.8% during the reaction. Propylene selectivity of HZ-AT increases from an initial 23.1% to a final 37.9%, ethylene selectivity decreases from 16.5 to 12.4%, and methane selectivity decreases to about 3.0%. The propylene selectivity increases from 28.0 to 47.6% for HZ-F2-AT, and it shows a higher $C_2^=-C_4^=$ selectivity. HZ, HZ-AT, and HZ-F2-AT exhibit increasing propylene selectivity and decreasing ethylene selectivity without reaching a steady state. HZ-F6-AT and HZ-F8-AT have a higher initial propylene selectivity of 39.0 and 41.1%, respectively, and both reach steady state after 50 h of reaction. HZ-F6-AT has the highest propylene selectivity of 50.5% at steady state. Table 3 shows average product selectivity during MTP reaction. Parent HZ has an especially high methane selectivity, which may be related to the poor diffusion rate that leads to quick coke deposition. Parent HZ also shows the lowest propylene selectivity of 31.4% but a higher ethylene selectivity of 17.5%, which results in the lowest P/E ($S_{Propylene}/S_{Ethylene}$) ratio of 1.8. HZ-AT, with its enclosed hierarchical structure, displays a slightly higher propylene selectivity of 33.6% due to minor enhancement of the diffusion rate. Larger acidity leads to much greater aromaticity than HZ. The lower amount of methane may be ascribed to the hollow structure and presence of less defect sites. Sequential treatment results in a significant increase of propylene selectivity. HZ-F6-AT, with its interconnected mesopore structure, shows the highest propylene selectivity

Table 3. Product Selectivity of Samples by Various Treatment Methods[a]

catalysts	selectivity (mol %)						P/E
	CH_4	C_2H_4	C_3H_6	$C_{2-4}^=$	C_{2-4}	C_5^+	
HZ	6.9	17.5	31.4	63.2	9.3	20.6	1.8
HZ-AT	2.4	13.8	33.6	63.7	9.6	24.3	2.4
HZ-F2-AT	2.4	15.1	43.1	70.2	9.3	18.1	2.9
HZ-F4-AT	1.5	13.4	44.8	70.3	9.4	18.8	3.3
HZ-F6-AT	1.5	10.9	48.8	72.0	8.7	17.8	4.5
HZ-F8-AT	1.4	11.0	47.2	69.2	9.3	20.1	4.3

[a]Calculated by the average selectivity from initial time to the time when methanol conversion is around 90%.

(48.8%) and P/E ratio (4.5). As shown in Scheme 1, there are two reaction cycles running synchronously in the methanol-to-

Scheme 1. Two Mechanistic Cycles during MTH Reaction on ZSM-5 Catalysts[18]
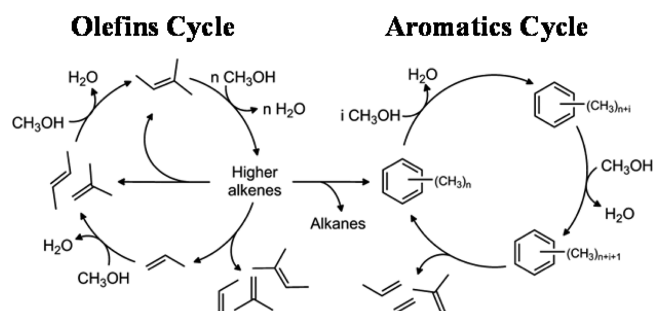
hydrocarbon process for ZSM-5 catalysts: an arene-based alkylation−dealkylation cycle and an olefin-based methylation-cracking cycle.[2,20,53] Ethylene and propylene can be generated by the aromatic-based cycle, whereas methylation/cracking involves only C2+ alkenes (without ethylene). Aditya Bhan et al. found that the resident time of aromatics in the pores reduced for crystals with smaller size, thus restricting its alkylation−dealkylation reactions before diffusing out of crystals that led to lower ethylene selectivity.[20] They also studied the catalytic performance of self-pillared ZSM-5 with a much higher diffusion rate. It showed much lower ethylene selectivity.[54] Introducing a mesoporous structure significantly weakened the proportion of aromatic-based reactions by shortening the resident time of aromatics; lower acidity also decreases the reactions between methylbenzene with active sites. Both of the two aspects lead to a much higher amount of propylene generated from a relatively increased number of olefin-based reactions for HZ-F6-AT, and it also shows a much lower methane and aromatic selectivity that may be attributed to a faster diffusion rate.

4. CONCLUSIONS

In summary, an open mesoporous structure, with a pore distribution centered around 13 nm, was introduced into Al-zoned ZSM-5 by a dealumination−realumination process during alkaline treatment. Also, single NaOH treatment selectively removed a larger amount of Si sites and hardly influenced the framework Al sites, thus leading to a lower Si/Al ratio and higher acidity. By contrast, a larger amount of Al sites were leached out for a higher concentration of NH₄F-modified samples in the initial stage during alkaline treatment (dealumination). Even though those Al in the filtrate were almost reinserted into zeolites in the final stage (realumination), the characterization results suggested less acidity of those reinserted Al sites, thus, the acidity of treated samples decreased with the increasing amount of participating Al in the dealumination−realumination process. HZ-F6-AT, with its interconnected hierarchical structure and suitable acidity, showed a longer lifetime of 195 h and a higher propylene selectivity of 48.8%. In contrast, single alkaline-treated ZSM-5 had an enclosed hollow structure and larger acidity, resulting in only a slightly increased lifetime (56 h) and propylene selectivity (33.6%) relative to the parent ZSM-5. The sequence of NH₄F and NaOH treatments allowed for integrated mesopore formation and acidity modification, bringing in a new method for controlled mesopore formation in Al-zoned ZSM-5 or high-silica zeolites. This method proved a significant step forward in MTP catalyst design with higher stability and selectivity.

■ ASSOCIATED CONTENT

ⓢ Supporting Information

The Supporting Information is available free of charge on the ACS Publications website at DOI: 10.1021/acsami.7b07806.

> ²⁹Si MAS NMR results of HZ and HZ-F6; TG-DTA results of different samples after deactivation; Comparative postmodification and catalytic results of fluorination-alkaline treatment based on ZSM-5 with homogeneous Al distribution (PDF)

■ AUTHOR INFORMATION

Corresponding Authors

*M.L.: Fax: +86 0411 84986134; E-mail: lium@dlut.edu.cn.

*C.S.: Fax: +1 814 863 4466; E-mail: csong@psu.edu.

ORCID Ⓞ

Min Liu: 0000-0003-2291-6266
Xinwen Guo: 0000-0002-6597-4979
Zhongmin Liu: 0000-0001-8439-2336
Chunshan Song: 0000-0003-2344-9911

Author Contributions

The manuscript was written through contributions of all authors. All authors have given approval to the final version of the manuscript.

Notes

The authors declare no competing financial interest.

■ REFERENCES

(1) Stöcker, M. Methanol-to-Hydrocarbons: Catalytic Materials and Their Behavior1. *Microporous Mesoporous Mater.* **1999**, *29*, 3−48.

(2) Olsbye, U.; Svelle, S.; Bjorgen, M.; Beato, P.; Janssens, T. V.; Joensen, F.; Bordiga, S.; Lillerud, K. P. Conversion of Methanol to Hydrocarbons: How Zeolite Cavity and Pore Size Controls Product Selectivity. *Angew. Chem., Int. Ed.* **2012**, *51*, 5810−5831.

(3) Bleken, F. L.; Chavan, S.; Olsbye, U.; Boltz, M.; Ocampo, F.; Louis, B. Conversion of Methanol into Light Olefins over ZSM-5 Zeolite: Strategy to Enhance Propene Selectivity. *Appl. Catal., A* **2012**, *447−448*, 178−185.

(4) Hu, Z.; Zhang, H.; Wang, L.; Zhang, H.; Zhang, Y.; Xu, H.; Shen, W.; Tang, Y. Highly Stable Boron-Modified Hierarchical Nanocrystalline ZSM-5 Zeolite for the Methanol to Propylene Reaction. *Catal. Sci. Technol.* **2014**, *4*, 2891−2895.

(5) Mei, C.; Wen, P.; Liu, Z.; Liu, H.; Wang, Y.; Yang, W.; Xie, Z.; Hua, W.; Gao, Z. Selective Production of Propylene from Methanol: Mesoporosity Development in High Silica HZSM-5. *J. Catal.* **2008**, *258*, 243−249.

(6) Lee, K.-Y.; Lee, S.-W.; Ihm, S.-K. Acid Strength Control in MFI Zeolite for the Methanol-To-Hydrocarbons (MTH) Reaction. *Ind. Eng. Chem. Res.* **2014**, *53*, 10072−10079.

(7) Chang, C. D.; Chu, C. T.-W.; Socha, R. F. Methanol Conversion to Olefins over ZSM-5. I. Effect of Temperature and Zeolite SiO2 Al2O3. *J. Catal.* **1984**, *86*, 289−296.

(8) Chu, C. T.-W.; Chang, C. D. Methanol Conversion to Olefins over ZSM-5. II. Olefin Distribution. *J. Catal.* **1984**, *86*, 297−300.

(9) Milina, M.; Mitchell, S.; Crivelli, P.; Cooke, D.; Pérez-Ramírez, J. Mesopore Quality Determines the Lifetime of Hierarchically Structured Zeolite Catalysts. *Nat. Commun.* **2014**, *5*, 3922−3931.

(10) Meng, X.; Yu, Q.; Gao, Y.; Zhang, Q.; Li, C.; Cui, Q. Enhanced Propene/Ethene Selectivity for Methanol Conversion over Pure Silica Zeolite: Role of Hydrogen-Bonded Silanol Groups. *Catal. Commun.* **2015**, *61*, 67−71.

(11) Teketel, S.; Skistad, W.; Benard, S.; Olsbye, U.; Lillerud, K. P.; Beato, P.; Svelle, S. Shape Selectivity in the Conversion of Methanol to Hydrocarbons: The Catalytic Performance of One-Dimensional 10-Ring Zeolites: ZSM-22, ZSM-23, ZSM-48, and EU-1. *ACS Catal.* **2012**, *2*, 26−37.

(12) Wei, F.-F.; Cui, Z.-M.; Meng, X.-J.; Cao, C.-Y.; Xiao, F.-S.; Song, W.-G. Origin of the Low Olefin Production over HZSM-22 and HZSM-23 Zeolites: External Acid Sites and Pore Mouth Catalysis. *ACS Catal.* **2014**, *4*, 529−534.

(13) Li, J.; Wei, Y.; Liu, G.; Qi, Y.; Tian, P.; Li, B.; He, Y.; Liu, Z. Comparative Study of MTO Conversion over SAPO-34, H-ZSM-5 and H-ZSM-22: Correlating Catalytic Performance and Reaction Mechanism to Zeolite Topology. *Catal. Today* **2011**, *171*, 221−228.

(14) Li, J.; Wei, Y.; Qi, Y.; Tian, P.; Li, B.; He, Y.; Chang, F.; Sun, X.; Liu, Z. Conversion of Methanol over H-ZSM-22: The Reaction Mechanism and Deactivation. *Catal. Today* **2011**, *164*, 288−292.

(15) Jamil, A. K.; Muraza, O.; Yoshioka, M.; Al-Amer, A. M.; Yamani, Z. H.; Yokoi, T. Selective Production of Propylene from Methanol

Conversion over Nanosized ZSM-22 Zeolites. *Ind. Eng. Chem. Res.* **2014**, *53*, 19498−19505.

(16) Liu, Z.; Dong, X.; Zhu, Y.; Emwas, A.-H.; Zhang, D.; Tian, Q.; Han, Y. Investigating the Influence of Mesoporosity in Zeolite Beta on Its Catalytic Performance for the Conversion of Methanol to Hydrocarbons. *ACS Catal.* **2015**, *5*, 5837−5845.

(17) Bjorgen, M.; Kolboe, S. The Conversion of Methanol to Hydrocarbons over Dealuminated Zeolite H-Beta. *Appl. Catal., A* **2002**, *225*, 285−290.

(18) Bjørgen, M.; Joensen, F.; Lillerud, K.-P.; Olsbye, U.; Svelle, S. The Mechanisms of Ethene and Propene Formation from Methanol over High Silica H-ZSM-5 and H-Beta. *Catal. Today* **2009**, *142*, 90−97.

(19) Tarach, K. A.; Tekla, J.; Makowski, W.; Filek, U.; Mlekodaj, K.; Girman, V.; Choi, M.; Góra-Marek, K. Catalytic Dehydration of Ethanol over Hierarchical ZSM-5 Zeolites: Studies of Their Acidity and Porosity Properties. *Catal. Sci. Technol.* **2016**, *6*, 3568−3584.

(20) Khare, R.; Millar, D.; Bhan, A. A Mechanistic Basis for the Effects of Crystallite Size on Light Olefin Selectivity in Methanol-to-Hydrocarbons Conversion on MFI. *J. Catal.* **2015**, *321*, 23−31.

(21) Koempel, H.; Liebner, W. Lurgi's Methanol to Propylene (MTP®) Report on a Successful Commercialisation. In *Natural Gas Conversion VIII*; Noronha, F., Schmal, M., Sousa-Aguiar, E. F., Eds.; Studies in Surface Science and Catalysis; Elsevier: Amsterdam, Netherlands, 2007; Vol. *167*, pp 261−267.

(22) Milina, M.; Mitchell, S.; Cooke, D.; Crivelli, P.; Perez-Ramirez, J. Impact of Pore Connectivity on the Design of Long-Lived Zeolite Catalysts. *Angew. Chem., Int. Ed.* **2015**, *54*, 1591−1594.

(23) Inagaki, S.; Sato, K.; Hayashi, S.; Tatami, J.; Kubota, Y.; Wakihara, T. Mechanochemical Approach for Selective Deactivation of External Surface Acidity of ZSM-5 Zeolite Catalyst. *ACS Appl. Mater. Interfaces* **2015**, *7*, 4488−4493.

(24) He, X.; Ge, T.; Hua, Z.; Zhou, J.; Lv, J.; Zhou, J.; Liu, Z.; Shi, J. Mesoporogen-Free Synthesis of Hierarchically Structured Zeolites with Variable Si/Al Ratios Via a Steam-Assisted Crystallization Process. *ACS Appl. Mater. Interfaces* **2016**, *8*, 7118−7124.

(25) Sheng, Y.; Zeng, H. C. Monodisperse Aluminosilicate Spheres with Tunable Al/Si Ratio and Hierarchical Macro-Meso-Microporous Structure. *ACS Appl. Mater. Interfaces* **2015**, *7*, 13578−13589.

(26) Möller, K.; Bein, T. Mesoporosity - a New Dimension for Zeolites. *Chem. Soc. Rev.* **2013**, *42*, 3689−3707.

(27) Shi, J.; Wang, Y.; Yang, W.; Tang, Y.; Xie, Z. Recent Advances of Pore System Construction in Zeolite-Catalyzed Chemical Industry Processes. *Chem. Soc. Rev.* **2015**, *44*, 8877−8903.

(28) Verboekend, D.; Pérez-Ramírez, J. Design of Hierarchical Zeolite Catalysts by Desilication. *Catal. Sci. Technol.* **2011**, *1*, 879−890.

(29) Wei, Y.; Parmentier, T. E.; de Jong, K. P.; Zecevic, J. Tailoring and Visualizing the Pore Architecture of Hierarchical Zeolites. *Chem. Soc. Rev.* **2015**, *44*, 7234−7261.

(30) Valtchev, V.; Majano, G.; Mintova, S.; Perez-Ramirez, J. Tailored Crystalline Microporous Materials by Post-Synthesis Modification. *Chem. Soc. Rev.* **2013**, *42*, 263−290.

(31) Triantafillidis, K. S.; Vlessidis, A. G.; Nalbandian, L.; Evmiridis, N. P. Effect of the Degree and Type of the Dealumination Method on the Structural, Compositional and Acidic Characteristics of H-ZSM-5 Zeolites. *Microporous Mesoporous Mater.* **2001**, *47*, 369−388.

(32) Groen, J. C.; Peffer, L. A.; Moulijn, J. A.; Perez-Ramirez, J. Mechanism of Hierarchical Porosity Development in MFI Zeolites by Desilication: The Role of Aluminium as a Pore-Directing Agent. *Chem. - Eur. J.* **2005**, *11*, 4983−4994.

(33) Zhang, H.; Hu, Z.; Huang, L.; Zhang, H.; Song, K.; Wang, L.; Shi, Z.; Ma, J.; Zhuang, Y.; Shen, W.; Zhang, Y.; Xu, H.; Tang, Y. Dehydration of Glycerol to Acrolein over Hierarchical ZSM-5 Zeolites: Effects of Mesoporosity and Acidity. *ACS Catal.* **2015**, *5*, 2548−2558.

(34) Groen, J. C.; Bach, T.; Ziese, U.; Paulaime-van Donk, A. M.; de Jong, K. P.; Moulijn, J. A.; Pérez-Ramírez, J. Creation of Hollow Zeolite Architectures by Controlled Desilication of Al-Zoned ZSM-5 Crystals. *J. Am. Chem. Soc.* **2005**, *127*, 10792−10793.

(35) Groen, J. C.; Zhu, W.; Brouwer, S.; Huynink, S. J.; Kapteijn, F.; Moulijn, J. A.; Pérez-Ramírez, J. Direct Demonstration of Enhanced Diffusion in Mesoporous ZSM-5 Zeolite Obtained Via Controlled Desilication. *J. Am. Chem. Soc.* **2007**, *129*, 355−360.

(36) Dai, C.; Zhang, A.; Liu, M.; Guo, X.; Song, C. Hollow Crystals: Hollow ZSM-5 with Silicon-Rich Surface, Double Shells, and Functionalized Interior with Metallic Nanoparticles and Carbon Nanotubes. *Adv. Funct. Mater.* **2015**, *25*, 7479−7487.

(37) Fodor, D.; Beloqui Redondo, A.; Krumeich, F.; van Bokhoven, J. A. Role of Defects in Pore Formation in MFI Zeolites. *J. Phys. Chem. C* **2015**, *119*, 5447−5453.

(38) Bjørgen, M.; Joensen, F.; Spangsberg Holm, M.; Olsbye, U.; Lillerud, K.-P.; Svelle, S. Methanol to Gasoline over Zeolite H-ZSM-5: Improved Catalyst Performance by Treatment with NaOH. *Appl. Catal., A* **2008**, *345*, 43−50.

(39) Mitchell, S.; Milina, M.; Verel, R.; Hernandez-Rodriguez, M.; Pinar, A. B.; McCusker, L. B.; Perez-Ramirez, J. Aluminum Redistribution During the Preparation of Hierarchical Zeolites by Desilication. *Chem. - Eur. J.* **2015**, *21*, 14156−14164.

(40) Liu, H.; Xie, S.; Xin, W.; Liu, S.; Xu, L. Hierarchical ZSM-11 Zeolite Prepared by Alkaline Treatment with Mixed Solution of NaOH and CTAB: Characterization and Application for Alkylation of Benzene with Dimethyl Ether. *Catal. Sci. Technol.* **2016**, *6*, 1328−1342.

(41) Verboekend, D.; Perez-Ramirez, J. Desilication Mechanism Revisited: Highly Mesoporous All-Silica Zeolites Enabled through Pore-Directing Agents. *Chem. - Eur. J.* **2011**, *17*, 1137−1147.

(42) Wang, D.; Zhang, L.; Chen, L.; Wu, H.; Wu, P. Postsynthesis of Mesoporous ZSM-5 Zeolite by Piperidine-Assisted Desilication and Its Superior Catalytic Properties in Hydrocarbon Cracking. *J. Mater. Chem. A* **2015**, *3*, 3511−3521.

(43) Yu, L.; Huang, S.; Miao, S.; Chen, F.; Zhang, S.; Liu, Z.; Xie, S.; Xu, L. A Facile Top-Down Protocol for Postsynthesis Modification of Hierarchical Aluminum-Rich MFI Zeolites. *Chem. - Eur. J.* **2015**, *21*, 1048−1054.

(44) Burel, L.; Tuel, A. Nanozeolites: New Strategies for Designing Ultra Small Silicalite Crystals with Very Few Framework Defects. *Microporous Mesoporous Mater.* **2013**, *174*, 90−99.

(45) Xu, T.; Zhang, Q.; Song, H.; Wang, Y. Fluoride-Treated H-ZSM-5 as a Highly Selective and Stable Catalyst for the Production of Propylene from Methyl Halides. *J. Catal.* **2012**, *295*, 232−241.

(46) Wang, Y.; Guo, X.; Zhang, C.; Song, F.; Wang, X.; Liu, H.-o.; Xu, X.; Song, C.; Zhang, W.; Liu, X.; Han, X.; Bao, X. Influence of Calcination Temperature on the Stability of Fluorinated Nanosized HZSM-5 in the Methylation of Biphenyl. *Catal. Lett.* **2006**, *107*, 209−214.

(47) Danilina, N.; Krumeich, F.; Castelanelli, S. A.; van Bokhoven, J. A. Where Are the Active Sites in Zeolites? Origin of Aluminum Zoning in ZSM-5. *J. Phys. Chem. C* **2010**, *114*, 6640−6645.

(48) Fodor, D.; Krumeich, F.; Hauert, R.; van Bokhoven, J. A. Differences between Individual ZSM-5 Crystals in Forming Hollow Single Crystals and Mesopores During Base Leaching. *Chem. - Eur. J.* **2015**, *21*, 6272−6277.

(49) Qin, Z.; Lakiss, L.; Tosheva, L.; Gilson, J.-P.; Vicente, A.; Fernandez, C.; Valtchev, V. Comparative Study of Nano-ZSM-5 Catalysts Synthesized in OH−and F−Media. *Adv. Funct. Mater.* **2014**, *24*, 257−264.

(50) Ma, D.; Shu, Y.; Zhang, W.; Han, X.; Xu, Y.; Bao, X. In Situ 1H MAS NMR Spectroscopic Observation of Proton Species on a Mo-Modified HZSM-5 Zeolite Catalyst for the Dehydroaromatization of Methane. *Angew. Chem., Int. Ed.* **2000**, *39*, 2928−2931.

(51) Barbera, K.; Bonino, F.; Bordiga, S.; Janssens, T. V. W.; Beato, P. Structure−Deactivation Relationship for ZSM-5 Catalysts Governed by Framework Defects. *J. Catal.* **2011**, *280*, 196−205.

(52) Sazama, P.; Wichterlova, B.; Dedecek, J.; Tvaruzkova, Z.; Musilova, Z.; Palumbo, L.; Sklenak, S.; Gonsiorova, O. FTIR and 27Al MAS NMR Analysis of the Effect of Framework Al- and Si-Defects in Micro- and Micro-Mesoporous H-ZSM-5 on Conversion of Methanol to Hydrocarbons. *Microporous Mesoporous Mater.* **2011**, *143*, 87−96.

(53) Ilias, S.; Khare, R.; Malek, A.; Bhan, A. A Descriptor for the Relative Propagation of the Aromatic- and Olefin-Based Cycles in Methanol-to-Hydrocarbons Conversion on H-ZSM-5. *J. Catal.* **2013**, *303*, 135−140.

(54) Khare, R.; Bhan, A. Mechanistic Studies of Methanol-to-Hydrocarbons Conversion on Diffusion-Free MFI Samples. *J. Catal.* **2015**, *329*, 218−228.